frontiers | Frontiers in Materials

TYPE Original Research
PUBLISHED 27 February 2025
DOI 10.3389/fmats.2025.1512695

OPEN ACCESS

EDITED BY
Annalisa Napoli,
University of Salerno, Italy

REVIEWED BY
Salvatore Verre,
University of eCampus, Italy
Xiaohua Li,
Chongqing University, China

*CORRESPONDENCE
Anandh Sekar,
anandhs@srmist.edu.in

RECEIVED 17 October 2024
ACCEPTED 16 January 2025
PUBLISHED 27 February 2025

CITATION
Mastan S, Sekar A and S. SN (2025) Effects of stiffener area in composite steel-concrete beam with web opening: numerical, experimental and theoretical investigation. *Front. Mater.* 12:1512695.
doi: 10.3389/fmats.2025.1512695

Effects of stiffener area in composite steel-concrete beam with web opening: numerical, experimental and theoretical investigation

Sheik Mastan, Anandh Sekar* and Sindhu Nachiar S.

Department of Civil Engineering, SRM Institute of Science and Technology, Kattankulathur, Tamil Nadu, India

Generally, the Openings in composite steel-concrete beams (CBs) for conduits and pipelines often compromise their flexural capacity. To mitigate this, longitudinal stiffeners (LS) and transverse stiffeners (TS) are strategically placed near the web openings. While previous research has explored various opening shapes and stiffener placements, limited studies have examined the impact of stiffener area on flexural performance. This study investigates the influence of stiffener area on the bending performance of composite beams with openings (CBOs). Numerical analysis using ABAQUS (v6.14) was conducted on beams with circular (CBC), rectangular (CBR), and triangular (CBT) openings, varying the breadth of stiffener (b) of LS and TS as 4 mm, 6 mm, 8 mm, and 10 mm. Results indicate that the ultimate load-carrying capacity of CBC with LS and TS increased from 290.50 kN (without stiffeners) to 375.56 kN, 383.46 kN, 387.42 kN, and 400.00 kN as the stiffener breadths were increased to 4 mm, 6 mm, 8 mm, and 10 mm, respectively, finally achieving a 37.6% improvement and comparable to 401.70 kN capacity of a beam without openings (CB). For CBR and CBT with the maximum breath of stiffener, the load-carrying capacities were 37% (380.50 kN) and 73% (336.86 kN) greater, respectively, compared to CBR and CBT without stiffeners. Thus, numerical results indicate that with an increase in the area of both stiffeners, the beam with openings exhibits an ultimate bearing capacity comparable to a beam without web openings. Further experimental investigation was performed on three specimens scaled down at a ratio of 1:0.32; here, the load-bearing capacity of the CBC with both stiffeners of the breath of 10 mm is 156.40 kN, which is 44% greater than the scaled-down CBC of 108.80 kN and comparable to the scaled-down CB's capacity of 151.12 kN. These experimental and numerical results emphasise that combining LS and TS with the maximum area of stiffeners, i.e., $l \times b$ (b = 10 mm), is most effective in maintaining the stability and load capacity of CBOs. Finally, the numerical and experimental results are validated against the theoretical results.

KEYWORDS

composite steel-concrete beam, web opening, area of stiffeners, FEM, load carrying capability

1 Introduction

A composite steel-concrete beam (CB) features a steel I-beam under tension, a concrete slab under compression, and shear connectors, ensuring the two materials are securely joined at their interface (Brozzetti, 2000; Queiroz et al., 2007; Ahmed, 2018; Papastergiou and Lebet, 2014; Shamass and Cashell, 2019; Ashraf et al., 2000; Liu et al., 2017; Peng et al., 2024). Thus, CB effectively maximizes the structural characteristics of steel and concrete. Compared to traditional steel or concrete beams used in isolation, this composite action significantly enhances the beam's load-carrying capacity, stiffness, and resistance to bending and deflection. By effectively distributing strains and stresses between the concrete and steel components, CB optimizes overall structural efficiency and durability, making it an advantageous solution for applications requiring high strength and minimal deformation in modern construction (Ahmed, 2018; Uy, 2016; Szewczyk and Szumigała, 2021; Ban and Bradford, 2013; Jun et al., 2018; Thomann and Lebet, 2008; Lin et al., 2014; Thevendran et al., 2000; Li et al., 2024). Web openings in composite beams (CBs) allow for integrating services such as electrical conduits and HVAC systems, facilitating greater versatile and efficient building designs. This arrangement can reduce the building's height and overall cost. However, these web openings can significantly alter stress distribution and load-carrying capacity, potentially affecting the beam's overall strength and stability (Rex Donahey et al., 1988; Fahmy, 1996; Manuel Benitez et al., 1998; Guo et al., 2023).

Over the past 30 years, various practical and theoretical studies have explored the behavior of CB with web openings (CBO) (Jun et al., 2018; Thomann and Lebet, 2008; Lin et al., 2014; Thevendran et al., 2000; Li et al., 2024; Rex Donahey et al., 1988; Fahmy, 1996; Manuel Benitez et al., 1998; Guo et al., 2023; Ellobody and Young, 2014; Al-Dafafea et al., 2019; DURIF et al., 2021; Mastan et al., 2024; Du et al., 2021; Ellobody and Young, 2016). Balaguru et al. (Tsavdaridis and Galiatsatos, 2015) examined the repercussions of web openings on the structural performance of CBs, using experimental methods to analyze stress distribution and load capacity, and reported a 15%–20% reduction in load-carrying capacity for CBO compared to CB. Garg et al. (Darwin, 1990) conducted a numerical investigation on CBO and found a 12% decrease in overall stiffness and a 30% increase in deflection for beams. Stress concentration factors were found to be 2.5 times higher around the corners of the openings. Ali et al. (Verre, 2022) concluded that CB with larger openings show increased deflection and deformation under applied loads, and common failure modes include shear failure near the openings and localized bending. Martin Classen et al. (Liu et al., 2016) conducted numerical analysis and stated that finite element models closely match experimental results, demonstrating the validity of the modelling approach. David M. Todd et al. (Dassault Systèmes, 2015) stated that composite sections with web openings have significantly higher bending strength than corresponding non-composite sections. Opening length, height, and eccentricity variations significantly affect the ultimate strength.

To enhance CBO load-bearing capacity, Ellobody and Young (2014) conducted a finite element study on CB featuring both reinforced and unreinforced web openings and revealed that CBO reinforced with horizontal stiffeners had a significantly enhanced load-carrying capacity compared to those with unreinforced web openings. Al-Dafafea et al. (2019) Horizontal stiffeners were the

TABLE 1 Previous studies in CBC with Stiffeners.

Author and year	Theme of research	Major findings
Mastan et al. (2024)	Numerical analysis through finite element modelling using ABAQUS is employed to investigate how different shapes of web openings	• Double-sided longitudinal and transverse stiffeners adjacent to circular openings offer performance comparable to conventional beams
Du et al. (2021)	Understanding and enhancing the flexural performance and load-bearing capacity of composite beams with reinforced web openings	• Web openings reinforced with longitudinal stiffeners significantly improved the ultimate bearing capacity • Transverse stiffeners provided minimal improvement in ultimate bearing capacity
Al-Dafafea et al. (2019)	Studied the mechanical behavior of steel beams with web openings	• Long horizontal stiffeners were the most effective solution for reinforcing web openings • Both single and double-sided stiffeners significantly improve the ultimate carrying capacity of the beams when the anchorage length is adequate
Ellobody and Young (2016)	Study on variations in stiffener configurations, web opening dimensions, and locations	• Stiffened web openings with horizontal stiffeners above and below openings significantly increases ultimate loads • Optimal opening height identified as 0.6 of steel beam depth
Tsavdaridis and Galiatsatos (2015)	study focuses on evaluating the structural behavior of cellular beams with transverse stiffeners	• The analysis showed that Vierendeel shearing failure occurred more often for closely spaced beam sections. • spacing between openings increased, the contribution of the stiffener to the strength of the beam reduced

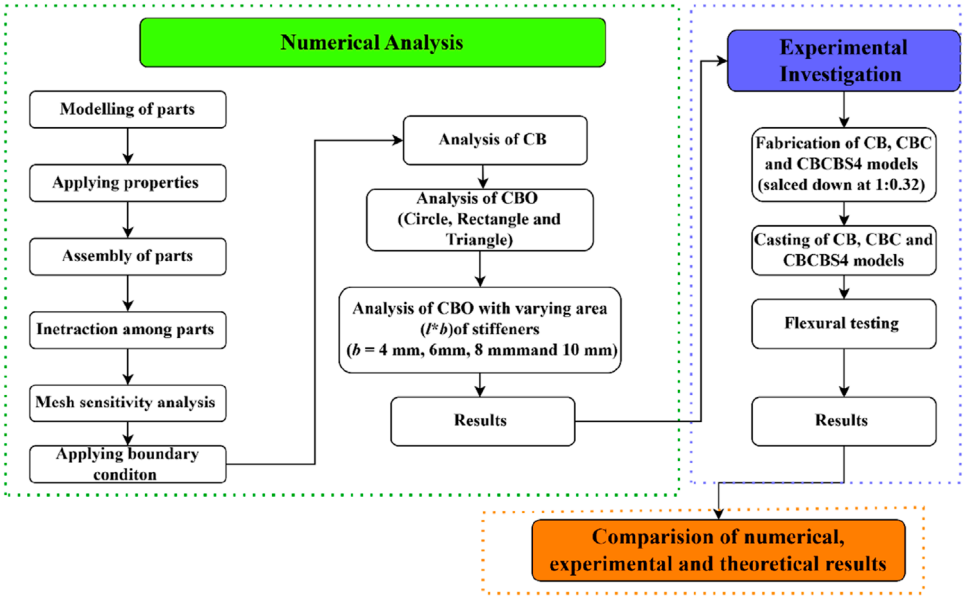

FIGURE 1
Diagram of methodology.

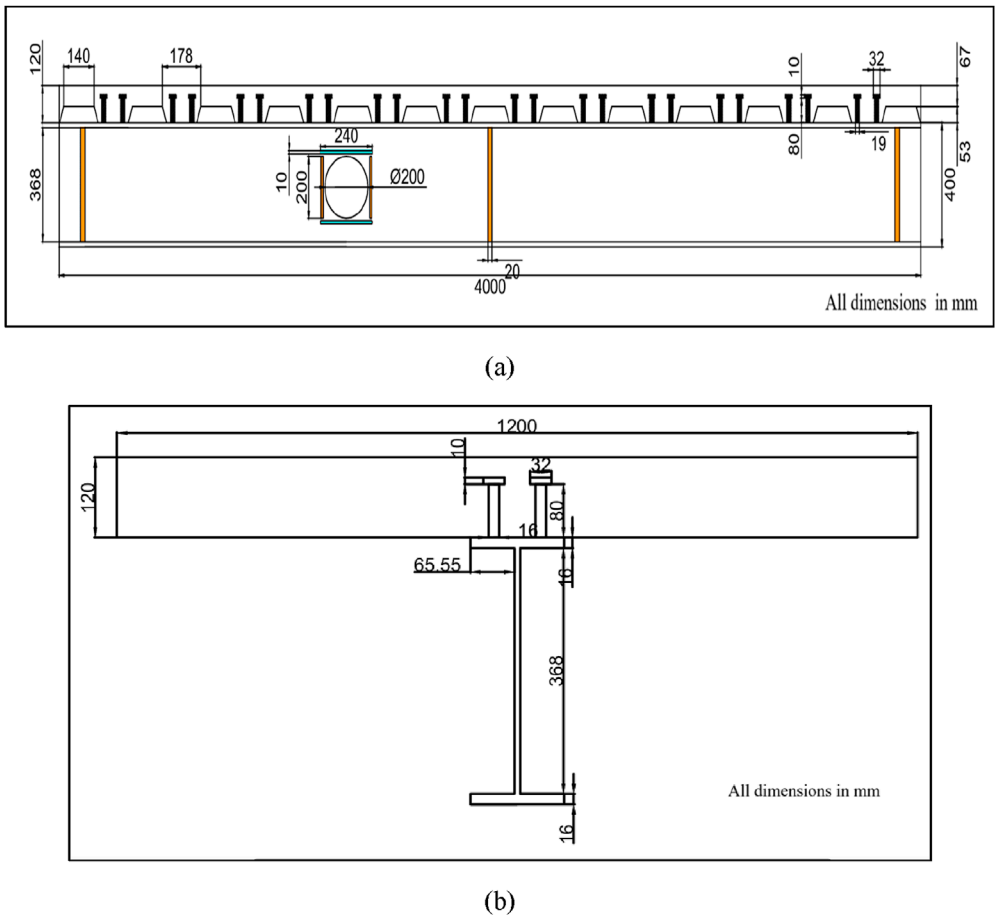

FIGURE 2
(A) CB Dimensions in mm. **(B)** Front Elevation in mm.

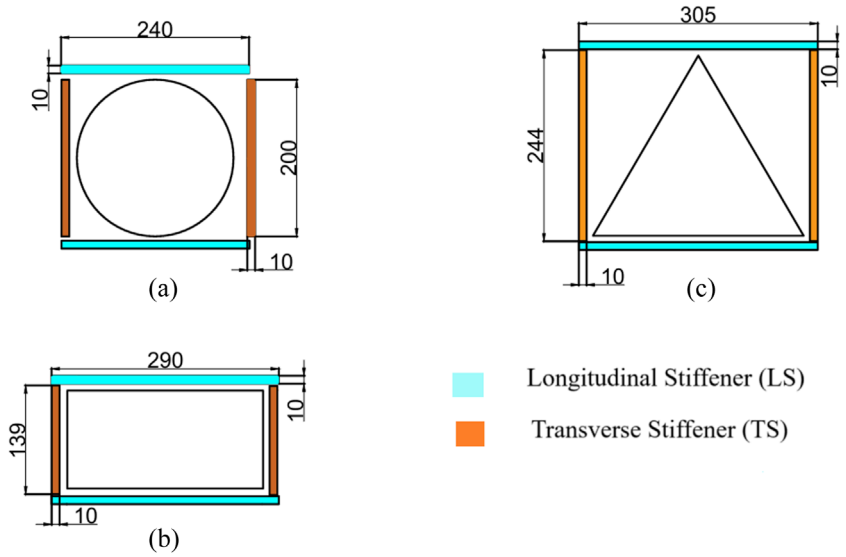

FIGURE 3
(A) CBCBS4. **(B)** CBRBS4. **(C)** CBTBS4.

TABLE 2 Details of the models.

Specimen	Position of stiffener	Area of stiffener (mm^2)		Model
		LS ($l_l \times b_l$)	TS ($l_t \times b_t$)	
Conventional composite beam	–	–		CB
CB with circular web opening	–	–		CBC
	LS and TS	120 × 4	200 × 4	CBCBS1
		120 × 6	200 × 6	CBCBS2
		120 × 8	200 × 8	CBCBS3
		120 × 10	200 × 10	CBCBS4
CB with rectangular web opening	–	–		CBR
	LS and TS	290 × 4	139 × 4	CBRBS1
		290 × 6	139 × 6	CBRBS2
		290 × 8	139 × 8	CBRBS3
		290 × 10	139 × 10	CBRBS4
CB with triangular web opening	–	–		CBT
	LS and TS	304 × 4	244 × 4	CBTBS1
		304 × 6	244 × 6	CBTBS2
		304 × 8	244 × 8	CBTBS3
		304 × 10	244 × 10	CBTBS4

[a] l_l = length of LS;*b_l = breath of LS;*l_t = length of TS;*b_t = breath of TS.

TABLE 3 Input properties.

Description	Shear connector	Reinforcement	Deck sheet	I-beam	Slab
Yield stress σy (N/mm^2)	326	670	282	310	–
Ultimate stress, σu (N/mm^2)	367	820	432	417	–
Modulus of elasticity	210,000				18,000
Density (kg/m^3)	7,800				2,400
Input parameters for defining the plastic behaviour					
Dilation angle (ψ)	Eccentricity (ξ)	Ratio of initial equibiaxial compressive yield stress to initial uniaxial compressive yield stress (σb0/σc0)	Second stress invariant on the tensile meridian to that on the compressive meridian (Kc)		Viscosity parameter (μ)
35	0.1000	1.1600	0.667		0.0005

TABLE 4 Concrete's physical properties.

Specimen	Cubic compression strength of concrete (MPa)			Average compressive strength of concrete (MPa)
CB	31.5	32.5	28.7	30.5
CBO	30.6	32.6	28.1	30.4
Optimised CBO	28.2	30.5	32.6	30.4

most effective, while short stiffeners showed limited benefits and could cause cracks. Monoliteral stiffeners enhanced global stiffness by 12% for high openings and 5% for smaller openings, while double-sided stiffeners improved it by 50%. Both stiffeners significantly enhanced ultimate strength, but strain distribution showed complexities beyond Vierendeel's theory, indicating the need for further finite element modelling. Evaluation of openings under local loads demonstrated differences in strength and behavior across opening shapes and stiffening methods, suggesting that current design codes may be overly conservative (Durif et al., 2021).

Few studies have investigated the flexural characteristics of CBOs strengthened with stiffeners, as shown in Table 1, as openings can potentially compromise composite beams' flexural performance and load-bearing capacity (CBs).

Mastan et al. (2024) conducted a study involving twenty-eight numerical models of reinforced web openings analysed under three-point bending. They concluded that CBOs with longitudinal stiffeners (LS) and transverse stiffeners (TS) can achieve a load-bearing capacity comparable to that of CBs. The present study performed numerical analyses with varying shapes of opening and stiffener areas, comparing CB and CB with circular, rectangular and triangular openings. Additionally, experimental tests were conducted on scaled CB, CBO, and an optimized model to predict ultimate bearing capacity.

2 Methodology

Numerical analysis has been carried out on CB, CBO, and CBOs with varying LS and TS areas. The steps involved in numerical analysis are presented in Figure 1. After obtaining the results from the numerical analysis, an experimental investigation was carried out on the optimised model, which was scaled down along with CB and CBC at a ratio of 1:0.32. Scaled-down models' fabrication and casting were carried out, respectively. Lastly, a numerical, experimental, and theoretical comparison was conducted. This process is illustrated in Figure 1.

3 Geometry

The CB is composed of a 4,000 mm-long ISMB 400 steel beam, a one mm-thick deck sheet, shear connectors 90 mm in length and 19 mm in width, and a concrete slab 120 mm thick and 1,200 mm wide. As specified in the AISC Steel Design Guide Series (Darwin, 1990), the stiffener must extend a distance $l_1 = \max\left(\frac{a_o}{4}; A_r\frac{\sqrt{3}}{2t_w}\right)$ Past the opening. Here A_r = the cross-sectional profile of the stiffener. The data above are depicted in Figure 2 with a circular-shaped opening with a diameter of 0.5D (where D = depth of the steel beam), positioned one-third of the span from the closest edge of the support.

The geometry of the stiffeners is described in two distinct types: LS and TS. The configurations and placement of these stiffeners adopted from BS EN 1994-1-1 are shown in the accompanying Figure 3, and detailed models are provided in Table 2. LS runs parallel to the beam's central axis, ensuring alignment along its length. TS are aligned orthogonally to the central axis, providing support across the width of the beam.

4 Numerical analysis

Finite Element Analysis (FEA) is widely used in civil engineering to model nonlinear behaviours of structures, such as masonry columns strengthened with composites. By incorporating material

TABLE 5 Details of scaled-down specimen.

Description	Steel profile								
	Upper tee (steel profile from top to mid-height)				Lower tee (steel profile from bottom to mid-height)				Length
	hwt (mm)	tw (mm)	bf (mm)	tf (mm)	hwb (mm)	tw (mm)	bf (mm)	tf (mm)	L (mm)
Numerical	184	8.9	140	16	184	8.9	140	16	4,000
Scaled-down (1:0.32)	58.8	2.8	44.8	5.1	58.8	2.8	44.8	5.1	1,280
Experimental	54.9	4.4	75	7.6	54.9	4.4	75	7.6	1,200

Description	Slab					Shear connector		Deck sheet
	b (mm)	H (mm)	hp (mm)	hc (mm)	f_{ck} (N/mm2)	h_d	d_d	t (mm)
Numerical	1,200	120	67	53	30	90	32	1
Scaled-down (1:0.32)	384	38.4	21.4	16.9	30	28.8	10.2	1
Experimental	400	40	23	17	30	31	20	1

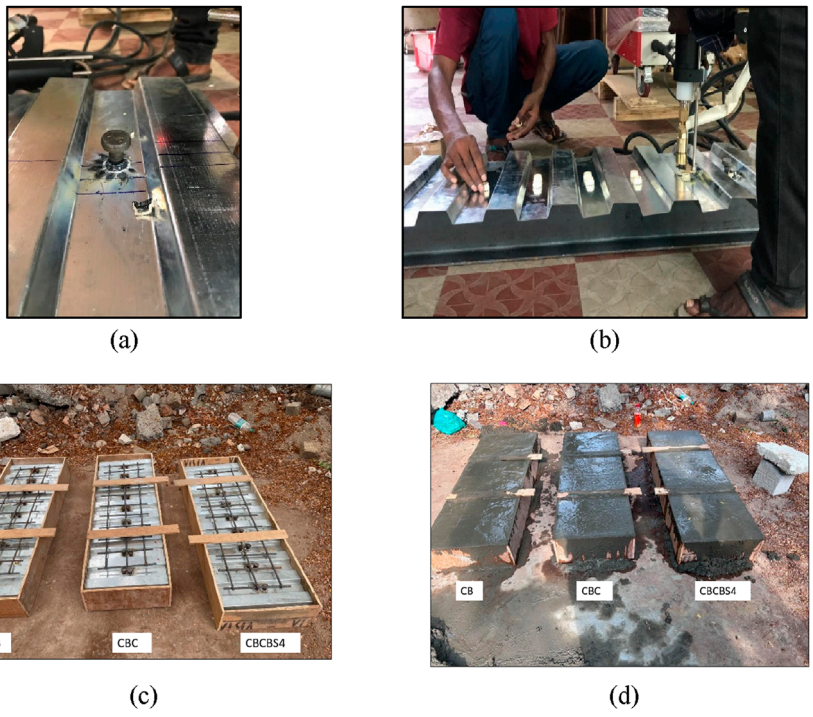

FIGURE 4
Fabrication of Specimen. **(A)** shear connector. **(B)** Arch Stud welding process. **(C)** Fabrication of CB, CBC and CBCBS4. **(D)** Casting of CB, CBC and CBCBS4.

properties from tensile coupon tests, FEA helps accurately predict structural performance and failure mechanisms under different loading conditions (Verre, 2022).

The maximum capacity of the specimens was evaluated using nonlinear analysis using the dynamic implicit method (Liu et al., 2016). The CB was discretised using solid elements (C3D8R) for the concrete slab, head stud, and steel beam, truss elements (T3D2) for reinforcement, and shell elements (S4) for the deck sheet, respectively (Dassault Systèmes, 2015; Hibbitt et al., 2011; Dong et al., 2021; Numerical et al., 2023; Wang et al., 2019; Hanbing et al., 2010). Based on the material evaluations, Table 3 presents the mechanical attributes of the components in the CB. Tensile

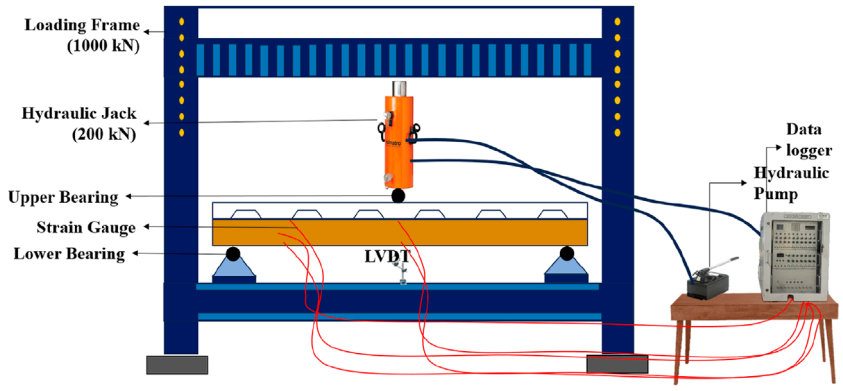

FIGURE 5
Schematic diagram of Experimental test setup.

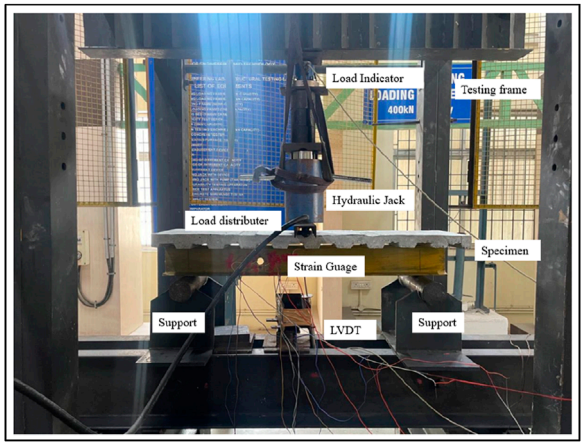

FIGURE 6
Experimental test setup.

coupon evaluations were performed to determine the ultimate tensile and yield strength of all elements except concrete, following ISO 6892–1 guidelines, as shown in Table 3 (Anon ISO 6892-1, 2016). As detailed in Table 4, three cube-shaped compression tests were performed on the concrete for the composite beam sample.

Further interaction among components of CB is assigned following Mastan et al. (2023), as depicted in Supplementary Figure S1. Surface-to-surface interaction is adopted between the steel beam and deck sheet, deck sheet and deck slab, shear connectors and steel beam, respectively. Embedded interaction is adopted for shear connectors and reinforcement in the deck slab.

Following a detailed mesh sensitivity analysis, the ideal element sizes for the model were established to optimise accuracy and computing performance. The mesh refinement procedure was performed in multiple critical zones, including the solid area, rib area of the concrete slab, reinforcement, head studs, deck sheet, and steel beam. Reducing the element size enhanced the accuracy of the results, especially in areas with significant stress gradients, such as around web openings and stiffeners. The investigation indicated that further refinement of the mesh above a specific threshold resulted in little enhancements in accuracy while substantially elevating computing expenses. Consequently, the ideal element sizes were chosen for their capacity to ensure consistent convergence while reducing computational expenditure. The final element dimensions were 80 for the solid region, 30 for the rib region in the concrete slab, 100 for reinforcement, 30 for head studs, 20 for the deck sheet, and 40 for the steel beam, as mentioned in Supplementary Figures S2, S3, ensuring the necessary precision and convergence in the model.

For applying the load and boundary condition, the model is supported by end A, which is pinned, and end B, which rests on a roller. A displacement of 10 mm per step is applied at the mid-span of the slab, which is represented by Supplementary Figures S4–S7. The loading and boundary conditions are also depicted in Supplementary Figure S4.

5 Fabrication of Specimen

The CB models were scaled down by a factor of 1:0.32 to maintain geometric similarity and proportion between the model and the prototype, as mentioned in Table 5, ensuring that the mechanical and structural properties of the system were accurately represented. Several key factors were considered when determining this scaling ratio.

- *True-to-Scale Proportions*: The 1:0.32 ratio was used to emulate the full-scale beam's section size, concrete slab dimensions, and span within feasible limitations. This scaling ratio guarantees that the scaled model preserves the relative geometry of the components, such as the steel beam, concrete slab, and shear connectors.
- *Geometric Compatibility*: The dimensions of the concrete slab were proportionately diminished to ensure compatibility between the steel beam and concrete slab in the scaled model. This ensured that both the steel and concrete elements were proportionately scaled, maintaining their interaction under load.

TABLE 6 Ultimate moment of the beam.

Description	Plastic neutral axis in the slab	Plastic neutral axis in the top flange of the beam	Plastic neutral axis in the web of the beam
Distance of neutral axis	$x = \frac{F_u}{f_c b_c} \le h_{c1}$	$y_1 = \frac{f_a A_{sn} + f_y A_r - F_u}{2 f_a b_f}$	$y_2 = \frac{f_a A_{sn} + f_y A_r - 2 f_a b_f - F_u}{2 f_a b_f} + t_f$
Ultimate bending moment	$M_m^I = \left(f_a A_{sn} + f_y A_r\right)\left(\frac{h_s}{2} + \frac{\Delta A_s e}{A_{sn}} + h_c - \frac{x}{2}\right)$	$M_m^{II} = \left(f_a A_{sn} + f_y A_r\right)\left(\frac{h_s}{2} + \frac{\Delta A_s e}{A_{sn}}\right) - f_a b_f y^2 + \left(h_c - \frac{h_{c1}}{2}\right)$	$M_m^{III} = \left(f_a A_{sn} + f_y A_r\right)\left(\frac{h_s}{2} + \frac{\Delta A_s e}{A_{sn}}\right) - f_a\left[t_w x^2 + \left(b_f - t_w\right) t_f^{\,2}\right] + F_u\left(h_c - \frac{h_{c1}}{2}\right)$

TABLE 7 FEM results of Models.

Models		Ultimate load (kN)	Ultimate deflection (mm)	Stress area (%)	Stiffness (kN/mm^2)
CB		401.70	55.20	6 0.00	8.1
Opening type		Circle			
CBC		290.50	30.70	15.90	6.00
CBC with LS and TS	CBCBS1	375.56	45.25	8.90	7.50
	CBCBS2	383.46	45.75	8.70	7.50
	CBCBS3	387.42	47.24	8.10	7.80
	CBCBS4	400.00	54.44	7.40	7.90
Opening type		Rectangle			
CBR		276.60	50.70	17.90	5.80
CBR with LS and TS	CBRBS1	368.56	45.26	10.90	5.50
	CBRBS2	376.32	45.75	11.40	6.10
	CBRBS3	377.20	47.25	11.50	6.10
	CBRBS4	380.50	59.40	11.80	6.40
Opening type		Triangle			
CBT		190.80	57.30	22.10	5.00
CBT with LS and TS	CBTBS1	320.02	29.68	13.10	5.30
	CBTBS2	326.76	30.00	13.40	5.50
	CBTBS3	330.13	30.98	13.70	5.40
	CBTBS4	336.86	32.61	14.80	5.50

- *Market Availability of Materials:* Practical factors, including material availability and the feasibility of manufacturing the reduced components, influenced the determination of the scaling factor. The ratio of 1:0.32 rendered the experimental configuration possible within the constraints of commercially obtainable materials for the scaled components.
- *Experimental Practicality:* The proportions of the scaled model were subsequently optimised according to experimental feasibility, taking into account equipment size restrictions and testing environment constraints. The chosen scaling ratio facilitated the experiment inside the limited space, ensuring that the materials and components were appropriately scaled to align with the testing conditions.

The stud connectors and deck sheet, as detailed in Table 5, are illustrated in Figure 4. The shear connectors are welded onto the steel beam using a stud arc welding machine, also shown in Figure 4. After welding, the reinforcement is attached, and the concrete is cast, as illustrated.

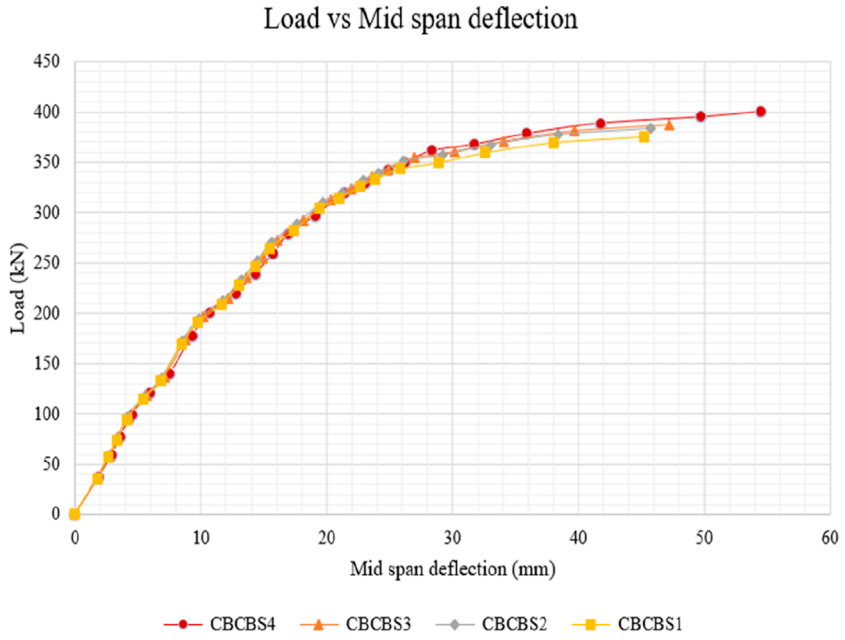

FIGURE 7
Load vs. Mid-span deflection for CBCBS1 to CBCBS4.

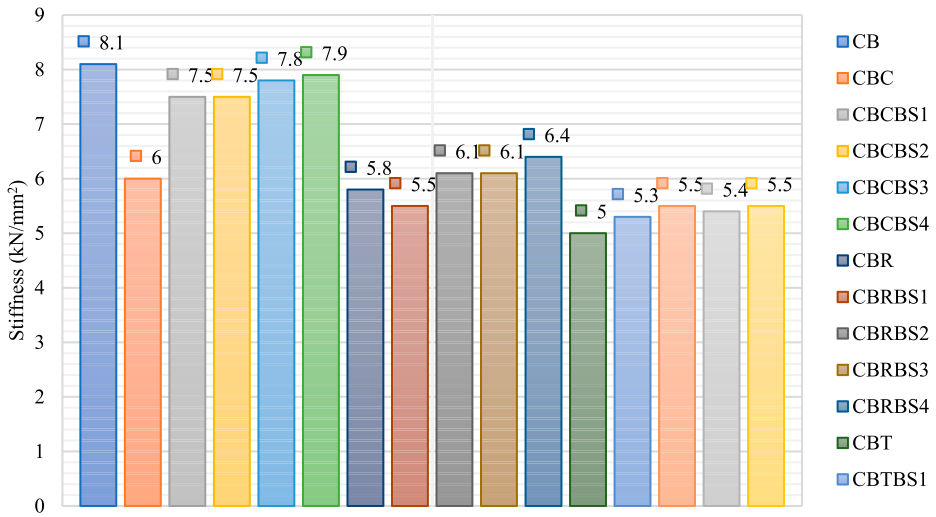

FIGURE 8
Stiffness of the models.

6 Experimental test setup

As illustrated in Supplementary Figure S9, the CB samples were subjected to three-point flexural testing using a high-capacity hydraulic actuator of 1,000 kN. To evaluate the effectiveness of the test arrangement, the CB samples were initially exposed to 10% of the estimated peak load applied at 0.5 kN/s and subsequently unloaded. The patterns of cracks and distortions around the opening in the web were monitored and documented after each loading stage. The load was subsequently raised by 5 kN increments until failure was observed. The ultimate load for the standard sample CB was calculated utilising the basic plastic analysis approach described in Eurocode 4 (BSI 2004 BS EN 1994, 2004).

For the CB specimen with web openings, the ultimate load was calculated using the approach outlined by Park et al. (2003)

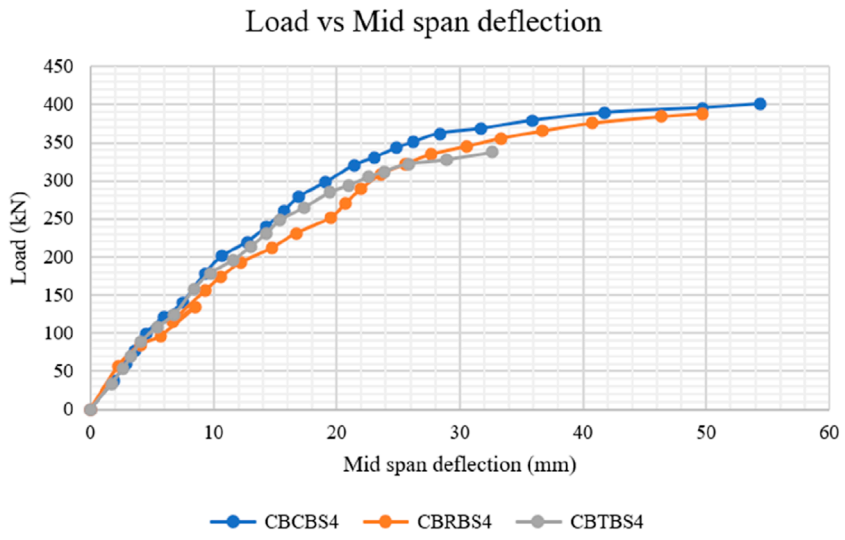

FIGURE 9
Load vs. mid-span deflection for CBCBS4, CBRBS4 and CBTBS4.

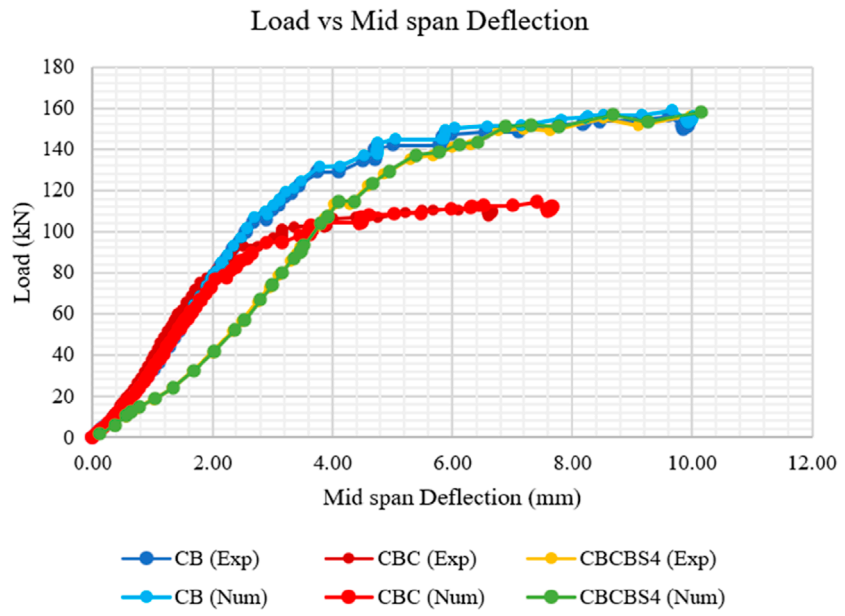

FIGURE 10
Load vs. mid-span deflection.

Supplementary Figure S10 and Figures 5, 6 illustrate the positioning of sensors and experimental arrangement for the CB specimens, respectively. LDVTs were deployed at mid-span to monitor the deflections of the CB during testing. The strain around the opening in the web was measured using a 45° strain gauge rosette. Additionally, six strain sensors were installed along the length of the LS to assess the strain pattern along these stiffeners. In contrast, four strain measurement devices were mounted on the TS as shown in Supplementary Figure S10.

The three-point flexural test was chosen for this study to directly assess the bending response of composite beams under concentrated loading conditions. This test configuration allows for precise evaluation of the beam's load-carrying capacity, deflection, and failure modes at mid-span, which is critical for understanding the structural behavior of composite beams with web openings and stiffeners. It was selected over alternative testing methods as it provides a clear and focused analysis of bending behavior with well-established data for comparison.

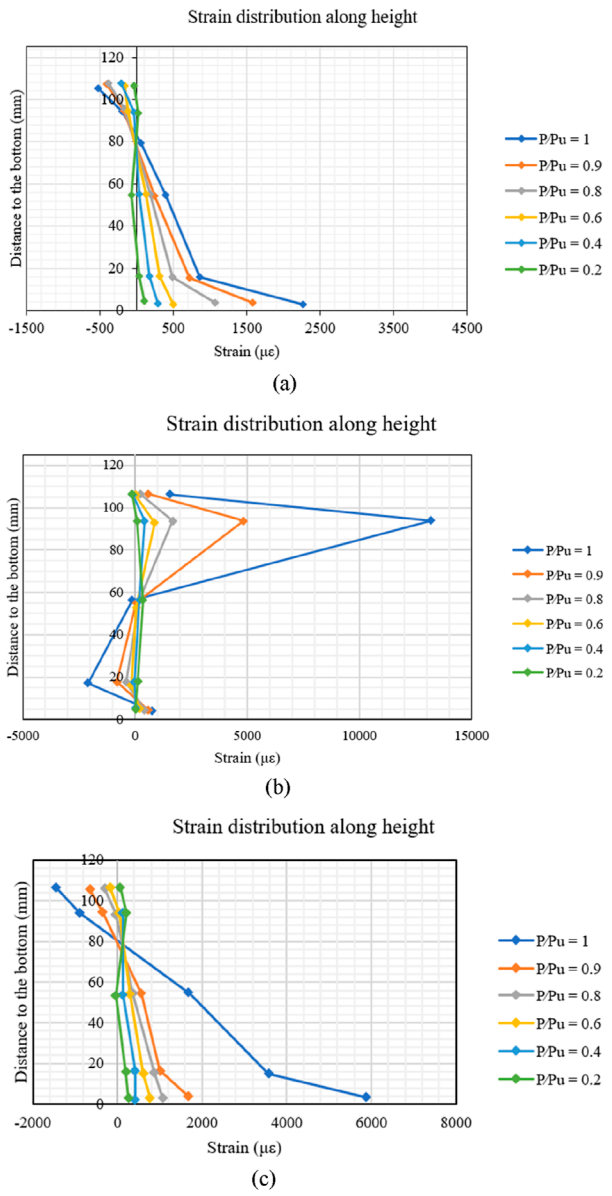

FIGURE 11
Strain distribution with the height of the steel section. **(A)** CB. **(B)** CBC. **(C)** CBCBS.

7 Theoretical investigation

From the ASCE (Concrete, 1992) a mathematical model is commonly used to evaluate the load-carrying capacity of CBs with openings on the web. The shear force and bending capacity at the centroid of the web opening were determined by analyzing the cumulative impact of shear force and bending moment. The bending capacity and shear force at the centroid of the web opening were determined by examining the combined effects of the bending moment (Du et al., 2021) and shear force (Du et al., 2021).

$$M_u = \varphi M_m \left[\left(\frac{M_m}{V_m \gamma} \right)^3 + 1 \right]^{\frac{-1}{3}} \quad (1)$$

$$V_u = \varphi V_m \left[\left(\frac{V_m \gamma}{M_m} \right)^3 + 1 \right]^{\frac{-1}{3}} \quad (2)$$

M_u = maximum bending moment;
V_u = maximum shear capacity
M_m = nominal bending moment at the centroid of web opening;
V_m = nominal shear force at the centroid of web opening;
φ = factored shear force at the centroid of web opening = 0.85 for CB

Structural analysis allows for calculating the moment shear ratio ($\gamma = M/V$) relative to the centroid of the opening once its location is determined.

7.1 Ultimate bending moment at web opening with stiffeners

The axial force of the CB, F_u, considered as the lowest value from the compression ability of the deck slab as Equation 3, F_c, the load-bearing of the shear connector as Equation 4, V_s, and the radial force of the CB as Equation 5, F_s. Hence, the axial load as Equation 6 F_u can be computed using the following equation:

$$F_c = f_c b_e h_{c1} \quad (3)$$

$$V_s = nV_u \quad (4)$$

$$F_s = f_a A_{sn} + f_y A_r \quad (5)$$

$$F_u = min\{F_c; V_s; F_s\} \quad (6)$$

f_c = compressive
t = strenght of concrete;
b_e = Slab width;
h_{c1} = equivalent depth of concrete slab;
f_y = yeild strenght of of stiffener;
V_u = load capacity shear connectors;
f_a = yeild strenght of beam;
A_{sn} = cross – sectional area of a perforated beam;
A_r = stiffeners′ area
e = distance to centroid

The ultimate moment of the beam with the equation is presented in Table 6. The conditions are as follows: the neutral axis is in the slab, top flange, and web of the beam. These conditions of the beam are illustrated in Supplementary Figure S12.

7.2 Maximum shear for CB with stiffener

The web and the accompanying stiffeners mainly sustained the shear loads on the I beams, whereas the contribution of the flange of the I beam in shear was disregarded. The shear capacities of the lower I beam (V_b) as in Equations 7, 10 and the upper I beam as in Equations 7–9 (V_t) Together, they make up the shear capacity of the CB (with a strengthened web opening). The shear strength of the upper and lower I beam is assessed by analyzing the relationship between normal stress and shear stress. The formula evaluates the

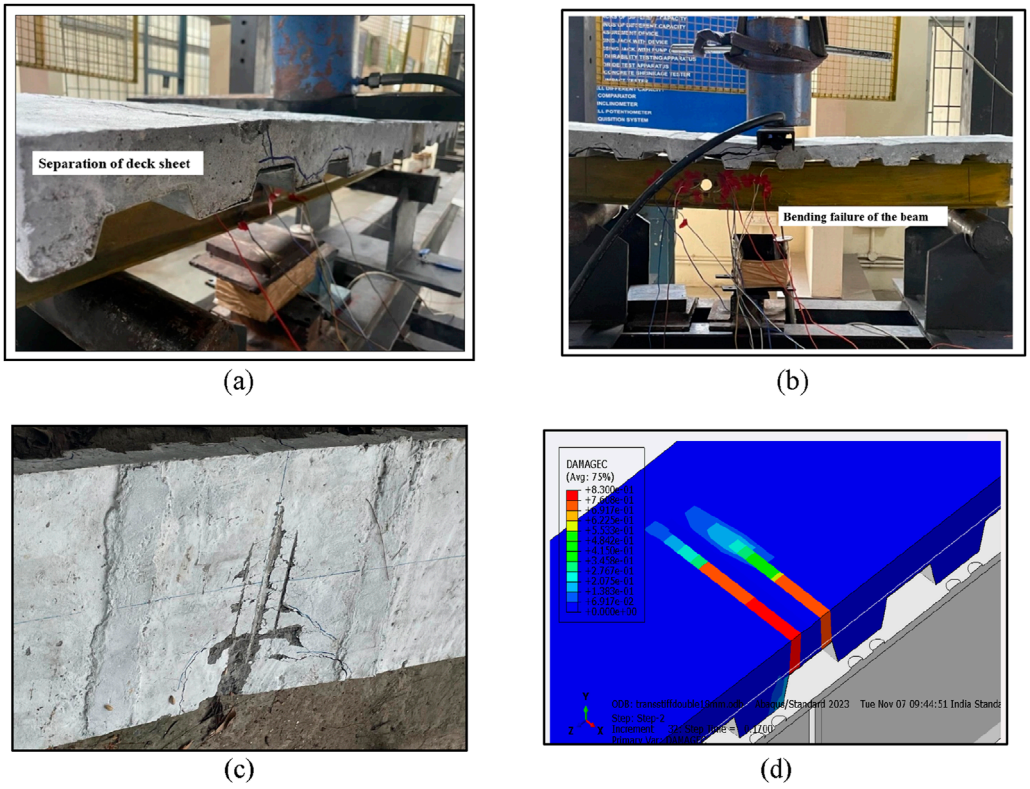

FIGURE 12
Experimental investigation. **(A)** separation of deck sheet and concrete slab. **(B)** Bending failure of the specimen. **(C)** Cracking pattern in experimental investigation. **(D)** Cracking pattern in numerical investigation.

TABLE 8 Comparison between experimental and numerical results.

Specimen	F_y/kN		Δy/mm		F_u/kN		Δu/mm		Mode of failure
	Ex	Nu	Ex	Nu	Ex	Nu	Ex	Nu	
CB	95.12	97.32	2.45	2.57	151.12	155.17	9.94	10.01	bending failure
CBC	68.48	68.91	1.64	1.89	108.80	110.01	6.65	7.71	shear failure
CBCBS4	92.02	94.56	3.46	3.67	156.40	158.51	9.98	10.16	bending failure

Ex*= experimental; Nu*= numerical.

shear resistance of the CB with a stiffened web opening:

$$V_m = V_t + V_b \tag{7}$$

$$V_t = \frac{\sqrt{2} f_a' h_t^2 t_w + f_y A_{rt} d_{rt} + F_{ch} d_h - F_{c1} d_s}{b_o + \sqrt{3} h_t} \tag{8}$$

$$V_t = \frac{\sqrt{6} + \mu}{\vartheta + \sqrt{3}} V_{pt} \tag{9}$$

With $V_{pt} = \frac{f_a t_w h_s}{\sqrt{3}}; \mu = \frac{f_y A_{rt} d_{rt} + F_{ch} d_h - F_{c1} d_s}{V_{pt}\left(h_t - \frac{f_y A_{rt}}{4 f_a b_f}\right)}; \vartheta = \frac{b_o}{h_t - \frac{f_y A_{rt}}{4 f_a b_f}}$ Where V_t = shear capacity of upper steel beam, h_t = height of upper steel beam, t_w = thickness of steel web, d_{rt} = distance from top to stiffener edge.

Shear capacity of lower steel beam.
Correspondingly,

$$V_b = \frac{\sqrt{2} f_a h_t^2 t_w + f_y A_{rt} d_{rb}}{b_o + \sqrt{3} h_b} \tag{10}$$

where: V_b = shear capacity of the lower steel beam.

8 Results and discussion

Finite element results, experimental results and theoretical results are compared, and findings are presented in this section.

TABLE 9 Comparison of experimental and theoretical results.

Specimen	V_u/kN		M_u/kN		V_u Exp/Theo
	Exp	Theo	Exp	Theo	
CB	90.67	90.72	45.33	46.76	0.99
CBC	64.10	66.10	32.64	33.05	0.98
CBCBS4	93.84	95.28	46.92	47.64	0.98

Ex*= experimental; Theo*= theoretical.

8.1 Numerical results

Numerical simulation was performed on all beams. The analysis predicted the Vonmises stress, peak principal stresses, fracture patterns, and deformation. Supplementary Figure S13 illustrates the maximum principal stress and deflection for the CB, respectively. In a similar manner, result plots for the other CBs were produced, and the data were compiled in Table 7.

Adding reinforcement adjacent to the opening alleviates stress intensification relative to composite beams without such openings. The stress region of each CB was measured and recorded using ImageJ software. Subsequently, the data regarding the ultimate load, ultimate deflection and stiffness of all models are presented in Table 7.

The data in Table 7 indicates that structural capacity is reduced by including an opening. Creating an opening within the CB results in a shift in stress distribution, which increases stress concentrations around the opening's perimeter, as depicted in Supplementary Figure S14. This concentration decreases the beam's total load-bearing capacity.

8.1.1 Effect of the area of stiffener on the opening

Among the models considered, the CBCBS4 model demonstrated a higher load-bearing capacity than the other models, as shown in Table 7. CBCBS4 achieved a load-bearing capacity of 400 kN, which is 6%, 4%, and 3% greater than CBCBS1, CBCBS2, and CBCBS3, respectively. Supplementary Figure S15, Figure 7 show the von Mises stress and the load vs. midspan deflection for these models.

Similarly, the CBRBS4 model reached a load-bearing capacity of 380.50 kN, surpassing CBRBS1, CBRBS2, and CBRBS3 by 3%, 1%, and 1%, respectively. Supplementary File 1 illustrates the load vs. midspan deflection for these models. Finally, the CBTBS4 model also achieved a load-bearing capacity of 336.86 kN, which is 5%, 3%, and 1% higher than CBTBS1, CBRBS2, and CBTBS3, respectively. Supplementary File 2 provides the load vs. midspan deflection for these models. This indicates that an increase in the area of the stiffener increases the load-bearing capacity of CB with web opening. The stiffness for all the models is illustrated in Figure 8, which indicates that openings reduce the stiffness of the models and stiffeners adjacent to openings increase the stiffness. Among the models with opening CBCS4, it attains higher stiffness.

8.1.2 Effect of shape of opening

The shape of the opening significantly influences the load-bearing capacity of a beam. Supplementary File 3 shows the load versus deflection for CBCBS4, CBRBS4, and CBTBS4. CBCBS4 attained a load-bearing capacity of 400.0 kN, which is 5% and 19% greater than CBRBS4 and CBTBS4, respectively. CBCBS4, CBRBS4, and CBTBS4 stiffness are measured at 7.9 kN/mm^2, 6.4 kN/mm^2, and 5.5 kN/mm^2, respectively. The percentage stress area around CBCBS4, CBRBS4, and CBTBS4 openings is 7.4%, 11.8%, and 14.8%, respectively. In summary, the beam with a circular opening and stiffeners on both sides performs better than beams with rectangular and triangular openings. Load vs. mid-span deflection for these models is illustrated in Figure 9.

8.2 Experimental and theoretical results

The following discussion outlines the experimental results for the scaled-down optimized models CB, CBC, and CBCBS4.

8.2.1 Load deflection behaviour

According to the experimental results, Figure 10 shows the correlations between the applied load and corresponding mid-span deflection in comparison with numerical results. During the initial loading phase, the CBs displayed linear elastic behaviour. As the applied force approached approximately 65% of the maximum load, the central deflection grew swiftly with the increasing stress while the bending rigidity of the CBs gradually reduced. During this phase, the load-displacement graph showed elastic-plastic characteristics. This was primarily due to increased slip between interfaces and the steel beam's lower flange yield. The empirical results revealed that the CB and CBCBS4 demonstrated a bending bearing capacity of 38% and 36.8% greater than the CBC, respectively. As soon as the section area of the double-sided LS and TS attained the compromised web opening area of the beam, the load-carrying capacity of the CBCBS4 was comparable to CB. The ultimate load-bearing capacity of CB, CBC and CBCBS4 is 151.12 kN, 108.80 kN, and 156.40 kN, respectively.

8.2.2 Strain behaviour pattern adjacent to the web opening

Figure 11 displays the strain dispersion throughout the vertical dimension of the steel section at the edges of the opening in the web. It was discovered that the steel section's strain dispersion was segmented and linear. Additionally, the hypothesis that the plane section would remain plane failed to hold here. The strain along the edges surrounding the opening was considerable in CBC, owing to the Vierendeel mechanism. Upon reaching the ultimate load, the shear stresses in the CBC exhibited a sudden increase due to significant shear distortion in the vicinity of the opening in the web. It was discovered that the strain in the region surrounding the opening was reduced due to the reinforcement provided by the stiffeners. The strain profiles of the CBs featuring reinforced web openings showed decreased variability. The primary factor was the effective constraint the stiffeners offered on the opening edges' distortions. The strain associated with the web opening in CBCBS4 decreased due to the reinforcement provided by the LS and TS. The primary factor was the collaborative interaction between the LS and

TABLE 10 Key findings from finite element and experimental.

Model	Analysis type	F_u/kN	Δu/mm	Stress area (%)	Stiffness (kN/mm^2)	Mode of failure	Remarks
CB	Num	401.70	55.20	6 0.00	8.1	Bending failure	–
	Num	155.17	10.01	5.81	15.51		Scaled-down
	Exp	**151.12**	**9.94**	–	**15.25**		
CBC	Num	290.50	30.70	15.90	6.00	shear failure	–
	Num	110.01	7.71	12.1	14.29		Scaled-down
	Exp	**108.80**	**6.65**	–	**14.30**		
CBCBS4	Num	400.00	54.44	7.40	7.90	Bending failure	–
	Num	158.51	10.16	6.12	15.69		Scaled-down
	Exp	**156.40**	**9.98**	–	**15.68**		
CBR	Num	276.60	50.70	17.90	5.80	shear failure	–
CBRBS4	Num	380.50	59.40	11.80	6.40		–
CBT	Num	190.80	57.30	22.10	5.00		–
CBTBS3	Num	330.13	30.98	13.70	5.40		–

Ex*= experimental; Num*= numerical. Here Bold values indicate the highest load-carrying capacity for each model configuration.

steel beam. The CBs with stiffened openings can effectively utilize the structural properties of both the LS and TS.

Figures 11A–C show the strain distribution along the height of the beam at various load levels (P/Pu). The strain patterns observed in these figures indicate the progressive variation in strain as the load increases. As the load approaches its maximum value (P/Pu = 1), strain near the bottom of the beam increases significantly, suggesting greater engagement of the lower regions in load-bearing. Conversely, the strain near the top remains lower, with the variation depending on the load level.

The strain distribution across the height indicates the beam's structural behavior under loading. Higher strain concentrations in certain regions, especially near the bottom, suggest areas under higher stress that could lead to potential failure or buckling. As strain variability increases, particularly at higher load levels, the beam's material properties are progressively engaged, with significant implications for structural stability. These strain patterns help understand the regions of maximum stress and guide the design to prevent overstressing any particular region, ensuring overall stability and optimal load distribution.

8.2.3 Experimental observations and modes of failure

The specimens CB and CBCBS exhibited consistent failure mode and analogous test results. At one-quarter of the ultimate load, horizontal fractures began forming near the centre of the CB. As the load increased to 65% of the maximum, Longitudinal fractures emerged in the middle of the concrete slab at the site of load application, as shown in Figure 12 with numerical counter-plot comparison, accompanied by transverse cracks at the support end. Subsequently, As the imposed load reached approximately 72% of the load-bearing limit, a diagonal fracture emerged in the concrete slab near the opening. It is illustrated in Figure 12, which compares the numerical results. As the load rose to 85% of maximum capacity, the deck sheeting started to marginally separate from the concrete, as shown in Figure 12. Upon reaching the ultimate load, the CBC experienced a failure due to pure shear at the web opening, which was attributed to the occurrence of four plastic hinges. In the case of the samples CB and CBCBS, noticeable gaps were detected between the deck and the concrete at the location of the opening, as shown in Figure 12. The steel web opening showed no visible damage.

The Table 8 presents the critical test results for CB, CBC, and CBCBS. Compared with the numerical results, these experimental findings reveal a significant deviation in the beam's behaviour under a concentrated load at the midpoint. In this table, F_y represents the load at which the lower flange of the steel beam yielded, gauged by strain gauges placed on the base flange of the steel beam. F_u denotes the peak load, while Δy was the mid-span deflection at the point when the lower flange yielded. Δu indicates the mid-span deflection upon reaching the maximum load.

The theoretical results are calculated using Equations 1, 2 in the theoretical investigation. The experimental and theoretical results are closely aligned and demonstrate a strong correlation, as shown in Table 9. The ratio of experimental and theoretical results of shear capacity is close to 1.0.

Table 10 summarises the key findings for each model, including ultimate load, ultimate deflection, stiffness, stress area, and mode of failure. It consolidates the results from finite element analysis and experimental calculations, offering a comparative overview of

the structural performance of composite beams with web openings and varying stiffener configurations. This summary facilitates the interpretation of the data and highlights the influence of stiffeners and opening shapes on the7 beam's load-bearing capacity and failure characteristics.

9 Conclusion

This investigation assessed the effects of the area of stiffeners on the reinforcement of web openings in composite beams. A total of 18 models with various types of stiffeners and web openings were analyzed. The optimized models were scaled down using a 1:0.32 ratio. Three specimens were then designed and subjected to three-point flexural tests. According to the findings, the following conclusions were derived.

- Among the different shapes of openings considered, circular openings attain high load-bearing capacity, high stiffness and low-stress area percentage compared to rectangular and triangular openings.
- Longitudinal and Transverse stiffeners with areas of 1,200 mm^2 and 2,800 mm^2, respectively, adjacent to the web opening increase the load-bearing capacity of the beam. Thus, CBCBS4 achieved a load-bearing capacity of 400 kN, i.e., 6%, 4% and 3% more than CBCBS1, CBCBS2, and CBCBS3, respectively.
- Similarly, CBRBS4 model reached a load-bearing capacity of 380.50 kN, surpassing CBRBS1, CBRBS2, and CBRBS3 by 3%, 1%, and 1%, respectively. The CBTBS4 model also achieved a load-bearing capacity of 336.86 kN, which is 5%, 3%, and 1% higher than CBTBS1, CBRBS2, and CBTBS3, respectively.
- Primary failure mode was identified in CB and CBCBS4: bending failure. The CBs with stiffeners near web openings showed favourable structural characteristics and enhanced flexibility.
- CBC failed in pure shear failure at the opening, characterised by the development of four plastic hinges and beam bending
- A combination of longitudinal and transverse stiffeners provides greater load-bearing capacity than CBC. CBCBS4 attained a 37% load-bearing capacity compared to CBC. Thus, it proved that CBC reinforced with LS and TS increases the load-bearing capacity of the beam.

Data availability statement

T7he original contributions presented in the study are included in the article/Supplementary Material, further inquiries can be directed to the corresponding author.

Author contributions

SM: Conceptualization, Formal Analysis, Investigation, Methodology, Software, Writing–original draft, Writing–review and editing. AS: Methodology, Supervision, Validation, Writing–review and editing. SS: Conceptualization, Methodology, Validation, Writing–review and editing.

Funding

The author(s) declare that no financial support was received for the research, authorship, and/or publication of this article.

Acknowledgments

The authors would like to acknowledge the Structural Testing Laboratory, Department of Civil Engineering, SRM Institute of Science and Technology, Kattankulathur

Conflict of interest

The authors declare that the research was conducted in the absence of any commercial or financial relationships that could be construed as a potential conflict of interest.

Generative AI statement

The author(s) declare that no Generative AI was used in the creation of this manuscript.

Publisher's note

Supplementary material

The Supplementary Material for this article can be found online at: https://www.frontiersin.org/articles/10.3389/fmats.2025.1512695/full#Supplementary-Material

References

Ahmed, F. D. (2018). *Behavior of composite beams with large web openings*. Egypt: Future University.

Al-Dafafea, T., Durif, S., Bouchaïr, A., and Fournely, E. (2019). Experimental study of beams with stiffened large web openings. *J. Constr. Steel Res.* 154, 149–160. doi:10.1016/j.jcsr.2018.11.026

Anon ISO 6892-1 (2016). *Metallic materials — tensile testing*. Part 1 Method test at room Temp.

Ashraf, A. B., Member, A., and Filippou, F. C. (2000). Mixed formulation of nonlinear steel-concrete composite beam element. *J. Struct. Eng.* 126, 371–381. doi:10.1061/(asce)0733-9445(2000)126:3(371)

Ban, H., and Bradford, M. A. (2013). Flexural behaviour of composite beams with high strength steel. *Eng. Struct.* 56, 1130–1141. doi:10.1016/j.engstruct.2013.06.040

Brozzetti, J. (2000). Design development of steel-concrete composite bridges in France. *J. Constr. Steel Res.* 55, 229–243. doi:10.1016/s0143-974x(99)00087-5

BSI 2004 BS EN 1994 (2004). *Structural use of steelwork in building — Part 4: code of practice for design of composite slabs with profiled steel sheeting*.

Concrete, T. A. (1992). Commentary on proposed specification for structural steel beams with web openings (with design example). *J. Struct. Eng.* 118, 3325–3348. doi:10.1061/(asce)0733-9445(1992)118:12(3325)

Darwin, D. (1990). *Steel and composite beams with web openings*. Steel Design Guide Series AISC-American Institute of Steel Construction.

Dassault Systèmes (2015). *Anon abaqus finite element analysis SIMULIA - dassault Systèmes*.

Dong, S., Guo, J., Zhang, C., An, X., and Lu, M. (2021). Finite element analysis on steel-concrete composite beams considering the bond-slip effect on the interface. *IOP Conf. Ser. Earth Environ. Sci.* 719, 022030. doi:10.1088/1755-1315/719/2/022030

Du, H., Hu, X., Shi, D., and Fang, B. (2021). Effect of reinforcement on the strength of the web opening in steel-concrete composite beam. *Eng. Struct.* 235, 112038. doi:10.1016/j.engstruct.2021.112038

Durif, S., Bouchair, A., and AL-Dafafea, T. (2021). Experimental study of various stiffened openings. *ce/papers*, 4, 1039–1047.

Ellobody, E., and Young, B. (2014). Behaviour and design of composite beams with stiffened and unstiffened web openings. *Adv. Struct. Eng.* 18, 6–32.

Ellobody, E., and Young, B. (2016). Behaviour and design of composite beams with stiffened and unstiffened web openings. *Adv. Struct. Eng.* 18, 893–918. doi:10.1260/1369-4332.18.6.893

Fahmy, E. H. (1996). Analysis of composite beams with rectangular web openings. *J. Constr. Steel Res.* 37, 47–62. doi:10.1016/0143-974x(95)00022-n

Guo, J., Shi, Q., Li, T., and Ma, G. (2023). Mechanical performance of hybrid high-strength steel composite cellular beam under low cyclic loading. *J. Constr. Steel Res.* 203, 107801. doi:10.1016/j.jcsr.2023.107801

Han-bing, L. I. U., Hui, M. A., Tian-ming, L. I. U., and Yun-long, ZHANG (2010). Analytical solution of steel-concrete composite beam under vertical loads. *china J. Highw. Transp.* 23, 39–44.

Hibbitt, H., Karlsson, B., and Sorensen, P. (2011). *Abaqus analysis users manual*. Providence Dassault Systemes Simulia.

Jun, S. C., Lee, C. H., Han, K. H., and Kim, J. W. (2018). Flexural behavior of high-strength steel hybrid composite beams. *J. Constr. Steel Res.* 149, 269–281. doi:10.1016/j.jcsr.2018.07.020

Li, X., He, J., Zhou, Y., Xu, F., Okazaki, T., and Fang, H. (2024). A comprehensive review of shear connectors in demountable composite beams. *J. Constr. Steel Res.* 218, 108723. doi:10.1016/j.jcsr.2024.108723

Lin, W., Yoda, T., Taniguchi, N., Kasano, H., and He, J. (2014). Mechanical performance of steel-concrete composite beams subjected to a hogging moment. *J. Struct. Eng.* 140, 04013031. doi:10.1061/(asce)st.1943-541x.0000800

Liu, X., Bradford, M. A., and Ataei, A. (2017). Flexural performance of innovative sustainable composite steel-concrete beams. *Eng. Struct.* 130, 282–296. doi:10.1016/j.engstruct.2016.10.009

Liu, X., Bradford, M. A., Chen, Q. J., and Ban, H. (2016). Finite element modelling of steel–concrete composite beams with high-strength friction-grip bolt shear connectors. *Finite Elem. Analysis Des.* 108, 54–65. doi:10.1016/j.finel.2015.09.004

Manuel Benitez, B. A., Darwin, D., Fellow, Z., and Donahey, R. C. (1998). Deflections of composite beams with web openings. *J. Struct. Eng.* 124, 1139–1147. doi:10.1061/(asce)0733-9445(1998)124:10(1139)

Mastan, S., Anandh, S., and Sindhu Nachiar, S. (2023). Numerical method and validation using ANN of composite steel–concrete beam for optimized geometry and emplacement of web opening. *Asian J. Civ. Eng.* 25, 1539–1559. doi:10.1007/s42107-023-00860-6

Mastan, S., Anandh, S., and Sindhu Nachiar, S. (2024). Performance of composite steel-concrete beam with stiffener next to web opening. *Eng. Res. Express* 6, 035112. doi:10.1088/2631-8695/ad6e56

Numerical, J., Editors, A., Wang, J., Nie, X., Zhao, H., Zhu, Y., et al. (2023). Numerical study on the effect of interface dynamic damage of steel–concrete composite beam bridge caused by high–frequency impact load. *Build. (Basel).* 13, 545. doi:10.3390/buildings13020545

Papastergiou, D., and Lebet, J. P. (2014). Design and experimental verification of an innovative steel–concrete composite beam. *J. Constr. Steel Res.* 93, 9–19. doi:10.1016/j.jcsr.2013.10.017

Park, J. W., Kim, C. H., and Yang, S. C. (2003). Ultimate strength of ribbed slab composite beams with web openings. *J. Struct. Eng.* 129, 810–817. doi:10.1061/(asce)0733-9445(2003)129:6(810)

Peng, F., Xue, W., and Bai, L. (2024). Flexural behavior of externally prestressed continuous steel-concrete composite beams. *J. Constr. Steel Res.* 212, 108282. doi:10.1016/j.jcsr.2023.108282

Queiroz, F. D., Vellasco, P. C. G. S., and Nethercot, D. A. (2007). Finite element modelling of composite beams with full and partial shear connection. *J. Constr. Steel Res.* 63, 505–521. doi:10.1016/j.jcsr.2006.06.003

Rex Donahey, B. C., Member, A., and Darwin, D. (1988). Web openings in composite beams with ribbed slabs. *J. Struct. Eng.* 114, 518–534. doi:10.1061/(asce)0733-9445(1988)114:3(518)

Shamass, R., and Cashell, K. A. (2019). Analysis of stainless steel-concrete composite beams. *J. Constr. Steel Res.* 152, 132–142. doi:10.1016/j.jcsr.2018.05.032

Szewczyk, P., and Szumigała, M. (2021). Optimal design of steel-concrete composite beams strengthened under load. *Materials* 14, 4715. doi:10.3390/ma14164715

Thevendran, V., Shanmugam, N. E., Chen, S., and Liew, J. Y. R. (2000). Experimental study on steel-concrete composite beams curved in plan. *Eng. Struct.* 22, 877–889. doi:10.1016/s0141-0296(99)00046-2

Thomann, M., and Lebet, J. P. (2008). A mechanical model for connections by adherence for steel–concrete composite beams. *Eng. Struct.* 30, 163–173. doi:10.1016/j.engstruct.2007.03.016

Tsavdaridis, K. D., and Galiatsatos, G. (2015). Assessment of cellular beams with transverse stiffeners and closely spaced web openings. *Thin-Walled Struct.* 94, 636–650. doi:10.1016/j.tws.2015.05.005

Uy, B. (2016). Applications, behaviour and design of composite steel-concrete structures. *Adv. Struct. Eng.* 15, 1559–1571. doi:10.1260/1369-4332.15.9.1559

Verre, S. (2022). Numerical strategy for column strengthened with FRCM/SRG system. *buildings* 12, 2187.

Wang, C., Shen, Y., Zou, Y., Zhuang, Y., and Li, T. (2019). Analysis of mechanical characteristics of steel-concrete composite flat link slab on simply-supported beam bridge. *KSCE J. Civ. Eng.* 23, 3571–3580. doi:10.1007/s12205-019-1921-1